High photosensitivity in SnO_2:SiO_2 optical fibres

G. Brambilla, V. Pruneri*, L. Reekie†,

Optoelectronics Research Centre, Southampton University, Southampton SO17 1BJ, U.K.

Fax: ++44 2380 593149, Tel: ++44 2380 593954, E-mail: gb2@orc.soton.ac.uk

* *Present address: Optical Technology Italia, Italy*

† *Present address: JDS Uniphase, Australia*

A. Paleari, N. Chiodini

Dipartimento di Scienza dei Materiali, I.N.F.M., University of Milano-Bicocca, via Cozzi 53, 20125 Milano, Italy

H. Booth

Oxford Lasers Ltd, Abingdon Science Park, Barton Lane, Abingdon, Oxon OX14 3YR, U.K.

Abstract

Enhanced photosensitivity has been achieved in tin-doped silica optical fibres. Refractive index modulations (~310^{-4}) have been achieved by use of 248 nm UV radiation. Studies performed on preform slides proved that the refractive index change can be ascribed to structural rearrangements induced by photochemical reactions. The modified structure has shown extreme stability and gratings written in this fibre start to be erased above 600 °C. Exposure of the fibre to 255 nm laser radiation showed that, at high fluence, the refractive index modulation saturates and does not exhibit any sign of decrease.

Introduction

Since its discovery in 1981 [1], fibre photosensitivity has been exploited to develop many applications such as in-fibre sensors, dispersion compensators and fibre laser mirrors. Telecom optical fibres exhibit small refractive index changes when exposed to UV radiation. Post-fabrication methods (such as hydrogen loading, flame brushing and thermal treatment) or co-doping are thus required to increase photosensitivity. B_2O_3 doping considerably increases photosensitivity but has significant drawbacks, such as high loss, high polarization mode dispersion and poor thermal stability of the grating. On the contrary, SnO_2 doping keeps the absorption in the telecom window at 1.5 μm low and induces little stress in the fibre. Moreover, gratings written in SnO_2 doped fibres show high thermal stability. SnO_2 has been used as a co-dopant to increase the photosensitivity of germano-silicate [2,3], phospho-silicate [4] and sodium-silicate optical fibres, and as a simple dopant in silica. SnO_2 co-doping has given high photo-induced refractive index modulations (Δn_{mod} ~10^{-3}) but at the expense of high NA [2,4]. In this work we give an overview of our studies on photosensitivity in SnO_2 doped silica, which shows not only considerable photosensitivity together with low NA, but also high thermal stability. In addition we used a 255 nm frequency-doubled Copper-vapour laser to write the gratings. This has allowed us to make a comparison with previous results obtained using a 248nm KrF excimer laser [5] and show that gratings can be written in this fibre with much shorter times using a higher pulse repetition rate source. Physical insights as to the mechanism behind photosensitivity have also been gained.

Fibre fabrication and Bragg grating writing

A major problem of tin silicate fibres is difficulty in fabrication, considering also the fact that crystallisation occurs for SnO_2 concentration <1 mol %. The SiO_2:SnO_2 fibres used

in the following experiments have been produced via modified chemical vapour deposition (MCVD). SnO_2 was introduced in the preform by bubbling O_2 through a $SnCl_4$ bubbler. The preform was fabricated by depositing a soot rich in SnO_2 at 1300 ^{0}C and then consolidating the sintered soot at 1800 ^{0}C. The collapse temperature was kept under 2200 ^{0}C to avoid massive SnO_2 volatilisation. In fact SnO_2 is extremely volatile and escapes from the glass layers during perform fabrication. Fig. 1 presents the preform refractive index profile. As a consequence of SnO_2 volatilisation during collapse, there is a large dip in the centre.

A fibre was produced from this perform, which had outer diameter OD~120 μm, numerical aperture (NA)~0.1 and cut-off wavelength (λ_c)~1.3 μm. Gratings ~4 mm long with high reflectivity at ~1543 nm were written using a KrF excimer laser and a phase-mask to create the interference pattern. This laser delivered pulses at 248 nm with duration ~20 ns, repetition rate (RR) 20 Hz and pulse fluence (I_p) ~80 mJ/cm^2. Fig. 2 shows the refractive index change induced in the fibre as a function of exposure time. The maximum refractive index modulation (Δn_{mod})~$2.8 10^{-4}$, corresponding to a reflectivity greater than 90%, was achieved after an exposure of 3.7 hours. Δn_{mod} was calculated by fitting the reflectivity curves (i.e. reflectivity R as a function of wavelength λ) using the following formulas:

$$R = \left(1 + \left(kL\,sinc\left(kL\sqrt{\delta^2 - 1}\right)\right)^{-2}\right)^{-1} \qquad (1)$$

$$k = \frac{\pi \Delta n_{mod}}{\lambda}$$

$$\delta = \frac{-2n_{av}}{\Delta n_{mod}\lambda_B}\left(\lambda - \lambda_B\right)$$

where L is the grating length, n_{av} the average refractive index, and $\lambda_B \sim 2\Lambda n_{av}$ the Bragg wavelength, Λ being the grating pitch.

Δn_{ave} was evaluated from the Bragg shift $\Delta\lambda_B$ according to the formula

$$\frac{\Delta n_{ave}}{n_{ave}} = \frac{\Delta \lambda_B}{\lambda_B} \quad (2)$$

Fig. 2 clearly shows that Δn_{mod} and Δn_{ave} have a similar evolution, as expected in type I gratings.

In GeO_2:SiO_2 optical fibres an equivalent Δn_{mod} under the same experimental conditions has been obtained only with [GeO_2]~10 mol % [6,7]. Standard telecom fibres (~ 4 mol % of GeO_2) produced Δn_{mod} one order of magnitude lower (~2.610^{-5}) [8]. It has also to be remarked that the dynamics of the grating growth are different. Grating growth in germanosilicate fibres is faster than in our experiments. In fact saturation was not achieved even after 3.7 hours exposure.

We also carried out experiments at a different wavelength using an Oxford Lasers' frequency doubled Cu vapour laser, working at 255 nm. Pulse duration, repetition rate and fluence were 20 ns, 6 kHz and 80 mJ/cm^2 respectively. Fig. 3 shows the time evolution of the ~3 mm long grating written in the same fibre using a phase mask. The reflection peak maximum was recorded in real time using a 50/50 coupler and a spectrum analyser. It can be observed that saturation is reached very quickly, due to the enormous fluence (i.e. high RR) delivered by the laser. Noteworthy is also the complete absence of type IIa gratings, observed in germano-silicate fibres at long exposures [9]. Once saturated, Δn_{mod} remains constant and does not show any decrease towards negative values. This different behaviour between SnO_2:SiO_2 and GeO_2:SiO_2 fibres can be explained by simply assuming that the photosensitivity in SnO_2:SiO_2 fibres is due to a single process and there are no other mechanisms that decrease Δn_{mod}(as observed in GeO_2:SiO_2).

To understand whether the photosensitive effect in SiO_2:SnO_2 glasses at 248 nm is driven by one- or multi-photon absorption, measurements at different UV laser intensities were carried out. If Δn_{mod} is assumed to have an initial growth proportional to the exposure

time (t) according to the law $I_p^{\beta} \cdot t$, then the numerical coefficient β is given by the slope of the growth rate $d(\Delta n_{mod})/dt$ vs I_p in a log-log plot. The photosensitivity is based on a one-photon process if β is close to 1 and it is multi-photon if β is 2 or greater. The dependence of $d(\Delta n_{mod})/dt$ on I_p is shown in ref [5]. β was evaluated to be ~0.99 confirming that the observed photosensitivity at 248 nm is governed by a single-photon absorption process [10].

Thermal stability of gratings

The thermal stability of the grating has been tested using an isochronal method to understand photosensitivity strength. The experimental set-up allowed in-situ measurements to be carried out. Light from a LED passed through a 50/50 coupler to the grating which was placed in a furnace. The reflected light was collected by an optical spectrum analyser through the coupler. The grating temperature was increased by a 45 ^{o}C step in 2 minutes and left at that temperature for ~28 minutes (fig. 4b). A reflection spectrum was recorded and the temperature step subsequently repeated. Fig. 4a summarises the temperature evolution of the grating spectra. Δn_{mod} for the different temperatures was evaluated by fitting the reflection spectra using eq. 1.

In fig. 5 measurements on fibres made of different materials are presented. The gratings in all of the fibres have been produced using a KrF excimer laser. The boro-germanosilicate fibre has shown the highest photosensitivity ($\Delta n_{mod} > 10^{-3}$) but the thermal stability of the grating was quite poor. The grating was completely erased at 550 ^{o}C. Gratings written in germano-silicate fibres showed lower photosensitivity but had a weaker decay. Nevertheless they still showed a gradual decrease in grating reflectivity for increasing temperature. On the contrary, the gratings written in SiO_2:SnO_2 fibres exhibited excellent

stability up to 600 °C and a sharp decrease in strength close to the erasure temperature. Assuming that Δn_{mod} is the result of a change in defect population [11], this last experimental observation can be explained assuming that the energy distribution of UV-induced defects is very narrow. Moreover the enhanced temperature stability indicates that potential wells associated to these traps are very deep. It is therefore difficult for the defect population to return to its original configuration. This feature might be helpful for the fabrication of devices that require operation at high temperatures or high intensities, where multi-photon processes can erase the photo-induced refractive index change.

In order to understand the origin of photosensitivity in tin-silicate fibres, we analysed the influence of UV exposure on slices from the same preform used to produce the fibre. In the next paragraph results obtained on the bulk sample are presented.

UV absorption and EPR spectra

Germano-silicate glasses show two main absorption peaks in the UV region: at 190 and 242 nm. Following UV exposure the 242 nm peak is bleached while the rest of the spectrum (the peak at 190 nm in particular) increases [12,13]. A commonly accepted model explains spectral modifications with defect reactions [14]: UV radiation bleaches germanium oxygen deficient centres (GODC) absorbing at 242 nm and produces three-fold coordinated Ge sites (GeE'), which increases the absorption at 190 nm. This defect is also paramagnetic, showing a strong electron paramagnetic resonance (EPR) signal at 343 mT, corresponding to a g-value of 2.001.

Figs. 6 and 7 respectively show UV absorption and EPR spectra of the preform used to produce the fibre whose properties are shown in fig. 1-4. The preform slice was polished on both sides down to 60 μm. The UV spectrum was recorded using a mask with a 500 μm

pinhole in order to analyse only the core area. It is clear from the figure that the spectrum of the unexposed sample is similar to that of a GeO_2:SiO_2 glass, with values comparable to those with 8 mol % of GeO_2 [8]. Note that the peak in the region 240-250 nm is shifted toward slightly longer wavelengths with respect to the germanosilicate UV spectrum. Recent measurements showed the possible substitutional role of Sn in the tetrahedral site of the SiO_2 network [15]. Sn atoms can produce defects that are typical of substitutional atoms in silica, like oxygen deficient or electronic related centres. We ascribe the absorption peak at 252 nm to the tin-oxygen deficient centre (Sn-ODC), analogous to the GODC absorbing at 242 nm in germano-silicate glasses. The 10 nm shift towards longer wavelengths with respect to the GODC is in agreement with the fact that the band-gap of SnO is lower than GeO.

The EPR spectrum presented in fig. 7 was recorded at room temperature with an EMX Bruker spectrophotometer operating at 9.6 GHz. The perform slice used had a thickness of 100 μm and was optically polished on both surfaces. Structures at 343.5, 345 and 347 mT, corresponding to g-values of 1.994, 1.984 and 1.976, have been identified with SnE' centres [16], consisting of an sp^3 unpaired electron of a three-fold coordinated Sn. The structure at 343 mT (g-value of 2.001) represents the signal of a SiE' centre.

We exposed the perform slide to the KrF excimer laser (I_p~100 mJ/cm^2, RR=20 Hz) and measured the absorption and EPR spectra after each exposure. The spectrum recorded after 300,000 pulses is shown in fig. 6 and UV-induced spectral variations at specific wavelengths are shown in the inset. In analogy with germano-silicate glasses, UV exposure clearly bleaches the peak at 252 nm and increases the absorption above 280 nm. The behaviour observed in the region below 210 nm is considerably different: in the SnO_2:SiO_2 preform negative absorption changes have been observed whereas in GeO_2:SiO_2 preforms the change is positive over the whole region 160-230 nm [6-8]. Fig. 7 shows the evolution of the

EPR spectrum after several UV exposures. Shifts along the vertical axis have been applied to emphasise spectral features. A clear growth of SnE' related signals can be observed. In addition, the growth of SnE' signal intensity as a function of UV exposure reproduces the behaviour of Δn_{mod}. SnE' centres formation might indicate that bond breaking in the neighbourhood of a Sn site is the initial step for network structural re-arrangements.

In germano-silicate glasses bleaching of the peak at 242 nm was associated with an increase of EPR signal associated with GeE' centres, indicating that UV laser radiation bleaches GODCs to produce GeE' sites [14]. Similarly, In analogy, from fig. 6 & 7 a similar dynamics can be observed: the bleaching of the 252 nm band indicates bond breaking at Sn-related defect sites, i.e. SnODC, with a resulting structural re-arrangement. The similar kinetics observed in figs. 6 and 7 suggests that the same kind of photoactivated mechanism is responsible for SnE' formation and Sn-ODC bleaching.

Although a Kramers-Kronig analysis performed on the absorption changes measured in GeO_2:SiO_2 preform slices corresponds to Δn_{mod} in fibres [6-8], UV spectral modifications in tin-silicate fibres have an opposite trend with respect to the refractive index change in the optical fibres. In fact absorption changes in the perform slice seem significantly small and mostly negative. Δn_{mod} in the perform slide, evaluated by applying Kramers-Kronig analysis to these absorption spectra, has a negative value at 1550 nm, in contrast to the fibre, where the value measured from Bragg grating experiments is positive (see fig.2).

Absorption measurements in the VUV have been performed below 190 nm down to the band-gap region [17] and show a similar behaviour to that observed in the range 190-280 nm. A general decrease in the absorption has been detected. A small increase has been detected only close to the band-gap edge. This is somewhat different from that observed in ordinary Ge-doped fibres, and suggests that the photorefractivity of Sn-doped silica glasses is

a more complex process. To clarify the structural modifications that take place in the perform when it is exposed to UV radiation and their relation to what happens in the optical fibre, we have carried out a wider analysis by means of micro-Raman mapping, photoluminescence (PL) measurements and stress polarimetry.

Raman spectroscopy and polarimetry

Several polished slices with thickness between 100 μm and 1 mm were exposed to an increasing number of pulses from the KrF laser (I_p~80 mJ/cm^2, RR~20 Hz). Micro-Raman spectroscopy has been carried out in a backscattering configuration using a Labram Dilor spectrometer. Excitation was produced in a spot of 3 μm^2 by using a HeNe laser or an Ar^+ laser.

Fig. 8 shows Raman spectra of the core and the cladding regions, respectively. The spectra show the characteristic broad band of amorphous SiO_2 between 400 and 500 cm^{-1}. The two narrow peaks D_1 and D_2 at ~490 and ~610 cm^{-1} are due, respectively, to the four-fold and three-fold planar rings of SiO_4 tetrahedra [18] that exhibit vibrational features completely uncoupled from the network. D_1 and D_2 peaks are representative of the medium-rande structural properties of pure silica and their intensities were observed to increase in densified silica [19]. In germano-silicate glasses, where Ge has a substitutional position, a decrease was observed by increasing the doping level [20]. In analogy, the large covalent dimension of Sn and its substitutional position in silica inhibit an optimum packing of the network. As a consequence, in the core the statistics of low order tetrahedral rings peaks (and thus the Raman signal) decreases. After laser exposure, no detectable change appeared in the Raman spectra. In contrast, in specific portions of the exposed preform a strong red luminescence dominated the collected spectra. This luminescence was attributed to non-bridging-oxygen

centres (NBO) [21] and was not observed in unexposed samples.

In ref. 22 we reported results on photoluminescence and stress birefringence on samples obtained from the same perform. The spatial distribution of PL induced by Sn-doping shows features completely different from the refractive index profile. PL centres are mainly distributed at the core-cladding interface and in the centre of the core, where the stress is higher. A stress birefringence map has been obtained with a polarimetric microscope working at the HeNe wavelength with two crossed polarisers and a quarter-wave plate. The results of the polarimetric analysis show that stresses are mostly present in doped regions and UV exposure induces a significant decrease of specific birefringence.

Physical mechanism for the enhanced photosensitivity

In tin-silicate glass, UV laser radiation in the 250 nm region is mainly absorbed by SnODCs, due to their intense peak in the absorption spectrum (fig. 6). We have shown how exposure to laser radiation bleaches SnODC, thus inducing compaction. Sn is introduced in the preform core in a substitutional position and forces the silica network into a less compact structure with respect to pure silica (fig. 8 shows the lower intensity of the D_1 and D_2 Raman modes). The bleaching of the 252 nm band (inset of Fig.6) and the increase of SnE' centres indicates the change of coordination properties of Sn sites, inducing a structural re-organization of the network in the Sn-doped part of the preform.Exposure also induces bond breaking in the stressed regions, like the core-cladding interface and the undoped centre. This is in agreement with the production of photo-luminescent NBO. As a result of these processes, in these areas the glass network becomes under–coordinated. The morphological constraints on the preform are released and the network can undergo structural modifications. The modified structure has an extremely deep and narrow potential well, showing excellent

temperature stability (fig. 5). Finally, in contrast to the behaviour of germanosilicate fibres, Δn_{mod} grows continuously until saturation is reached (fig. 3) indicating that competing mechanisms that would tend to decrease the refractive index are negligible.

Conclusions

In summary, significant photosensitivity has been achieved in SnO_2:SiO_2 optical fibres, even at a very low concentrations of SnO_2. The analysis of the effects of exposure to 248 nm laser radiation on preform slides showed that photosensitivity can be explained by structural rearrangements induced by photochemical reactions. The perturbed structure is extremely stable and the induced Δn_{mod} is erased only above 600 ^{o}C. Exposure to 255 nm laser radiation showed that Δn_{mod} grows continuously until saturation and no decrease at long exposure times has been observed.

G. Brambilla and V. Pruneri acknowledge Pirelli Cables for their studentship and fellowship respectively. This work was partially supported by the Ministero Italiano della Ricerca Scientifica.

References

1 Hill, K.O., Y. Fujii, D.C. Johnson, and B.S. Kawasaki. 1978. Photosensitivity in optical fiber waveguides: Application to reflection filter fabrication. Appl. Phys. Lett. 32(10): 647.

2 Dong, L., J.L. Cruz, L. Reekie, M.G. Xu, and D.N. Payne. 1995. Enhanced photosensitivity in tin-codoped germanosilicate optical fibers. IEEE Photonics Tech. Lett. 7(9): 1048.

3 Imamura, K., T. Nakai, Y. Sudo and Y. Imada. 1998. High reliability tin-codoped germanosilicate fibre Bragg gratings fabricated by direct writing method. Electron. Lett. 34(18): 1772.

4 Dong, L., J.L. Cruz, J.A. Tucknott, L. Reekie, and D.N. Payne. 1995. Strong photosensitive gratings in tin-doped phosphosilicate optical fibers. Optics Lett. 20(19): 1982.

5 Brambilla, G., V. Pruneri, and L. Reekie. 2000. Photorefractive index gratings in SnO_2:SiO_2 optical fibers. Appl. Phys. Lett. 76(7): 807.

6 Atkins, R.M., and V. Mizrahi. 1995. Observations of changes in UV absorption bands of singlemode germanosilicate core elliptical fibres on writing and thermally erasing refractive index gratings. Electron. Lett. 28(18): 1744.

7 Dong, L., J.L. Archambault, L. Reekie, P. St. J. Russell, and D.N. Payne.1995. Photoinduced absorption change in germanosilicate performs: evidence for the color-center model of photosensitivity. Appl. Opt. 34(18): 3436.

8 R.M. Atkins, V. Mizrahi, and T. Erdogan. 1993. 248nm induced vacuum UV spectral changes in optical fibre perform cores: support for a colour-centre model of photosensitivity. Electron. Lett. 29(4): 385.

9 Xie, W.X., P. Niay, P. Bernage, M. Douay, J.F. Bayon, T. Georges, M. Monerie, and B. Poumellec. 1993. Experimental evidence of two types of photorefractive effects occurring during photoinscriptions of Bragg gratings within germanosilicate fibers. Opt. Commun. 104(1-3): 185.

10 Albert, J., B. Malo, K.O. Hill, F. Bilodeau, D.C. Johnson, and S. Theriault. 1995. Comparison of one-photon and two-photon effects in the photosensitivity of germanium-doped silica optical fibers exposed to intense ArF excimer laser pulses. Appl. Phys. Lett. 67(24): 3529.

11 Erdogan, T., V. Mizrahi, P.J. Lemarie, and D. Monroe. 1994. Decay of ultraviolet-induced fibre Bragg gratings. J. Appl. Phys. 76(1): 73

12 Atkins, R.M., V. Mizrahi, and T. Erdogan. 1993. 248nm induced vacuum UV spectral changes in optical fibre perform cores: support for a colour centre model of photosensitivity. Electr. Lett. 29(4): 385.

13 Dong, L., J.L. Archambault, L. Reekie, P. St. J. Russel, and D.N. Payne. Photoinduced absorption change in germanosilicate performs: evidence for the color-center model of photosensitivity. Appl. Opt. 34(18): 3436.

14 Nishii, J., K. Fukumi, H. Yamanaka, K. Kawamura, H. Hosono, and H. Kawazoe. 1995. Photochemical reactions in GeO2-SiO2 glasses induced by ultraviolet irradiation: comparison between Hg lamp and excimer laser. Phys. Rev. B 52(3): 1661.

15 Chiodini, N., F. Morazzoni, A. Paleari, R. Scotti, and G. Spinolo. 1999. Sol-gel synthesis of monolithic tin-doped silica glass. J. Mater. Chem. 9: 2653.

16 Chiodini, N., F. Meinardi, F. Morazzoni, A. Paleari, R. Scotti, and G. Spinolo. 1998. Identification of Sn variants of the E' center in Sn-doped SiO2. Phys. Rev. B 58(15): 9615.

17 Anedda, A., C.M. Carbonaro, A. Serpi, N. Chiodini, A. Paleari, R. Scotti, G. Spinolo, G. Brambilla, and V. Pruneri. 2000. Vacuum ultraviolet absorption spectrum of photorefractive Sn-doped silica fiber performs. J. Non-Cryst. Sol. (to be published).

18 Pasquarello, A., and R. Car. 1998. Identification of Raman defect lines as signatures of ring structures in vitreous silica. Phys. Rev. Lett. 80(23): 5145.

19 Geissberger, A.E., and F.L. Galeener. 1983. Raman studies of vitreous SiO_2 versus fictive temperature. Phys. Rev. B 28(6): 3266.

20 Mukherjee, S.P., and S.K. Sharma. 1985. A comparative Raman study of the structures of conventional and gel-derived glasses in the SiO_2-GeO_2 system. J. Non-Cryst. Sol. 71(1-3): 317.

21 Skuja, L.. 1994. The origin of the intrinsic 1.9 eV luminescence band in glassy SiO_2. J. Non-Cryst Sol. 179: 51.

22 Chiodini, N., S. Ghidini, A. Paleari, G. Brambilla, and V. Pruneri, Photoinduced processes in Sn-doped silica fiber-preforms. Appl. Phys. Lett. to be published.

Figure captions

1. Refractive index profile in the tin doped perform. $[SnO_2]_{ave}$~0.15 mole %.

2. Growth of Δn_{mod} (empty circles) and Δn_{ave} (filled circles) resulting from exposure to KrF laser. The straight line represents the fit obtained with a stretched exponential. The grating length was 4 mm, pulse fluence and repetition rate were I_p~80 mJ/cm^2 and RR=20 Hz respectively.

3. Dependence of grating reflectivity on exposure time to Cu vapour laser. Grating length, laser pulse fluence and repetition rate were 3 mm, I_p~80 mJ/cm^2 and RR=6 kHz respectively.

4. a) Dependence of the grating spectrum on the temperature. b) Furnace thermal cycle: the sample was heated in steps of ~ 45 °C (starting from 205 °C) in 2 min per step and kept at that temperature for 28 min before the temperature was increased in another step.

5. Comparison between the temperature stability of gratings written in Boro-germanosilicate (SGB), germanosilicate (SG) and tin-silicate (SS) optical fibres.

6. UV absorption spectra of a SiO_2:SnO_2 optical preform slice (~60 μm thick) before (solid) and after (dashed) KrF excimer laser exposure (300,000 pulses, repetition rate RR=20 Hz, pulse fluence I_p~100 mJ/cm^2). Inset: UV induced absorption changes at 195,252 and 285 nm. The solid lines represent the fit obtained with stretched exponentials.

7. First derivative EPR spectrum of silica fiber preforms after different laser exposures in X-band at 300 K. Spectra of exposed samples have been translated in order to make the graph clear. Laser pulse fluence, repetition rate and pulse duration were I_p ~ 80 mJ/cm^2, RR~20 Hz and 20 ns respectively.

8. Raman spectra of the core and the cladding areas. The excitation laser is a Ar^+ ion at 514 nm focused on a surface of 3 μm^2. D_1 and D_2 are the peaks representative of 4-fold and 3-fold rings tetrahedra, ω_1, ω_3, and ω_4 the broad bands of vitreous silica.

Fig. 1

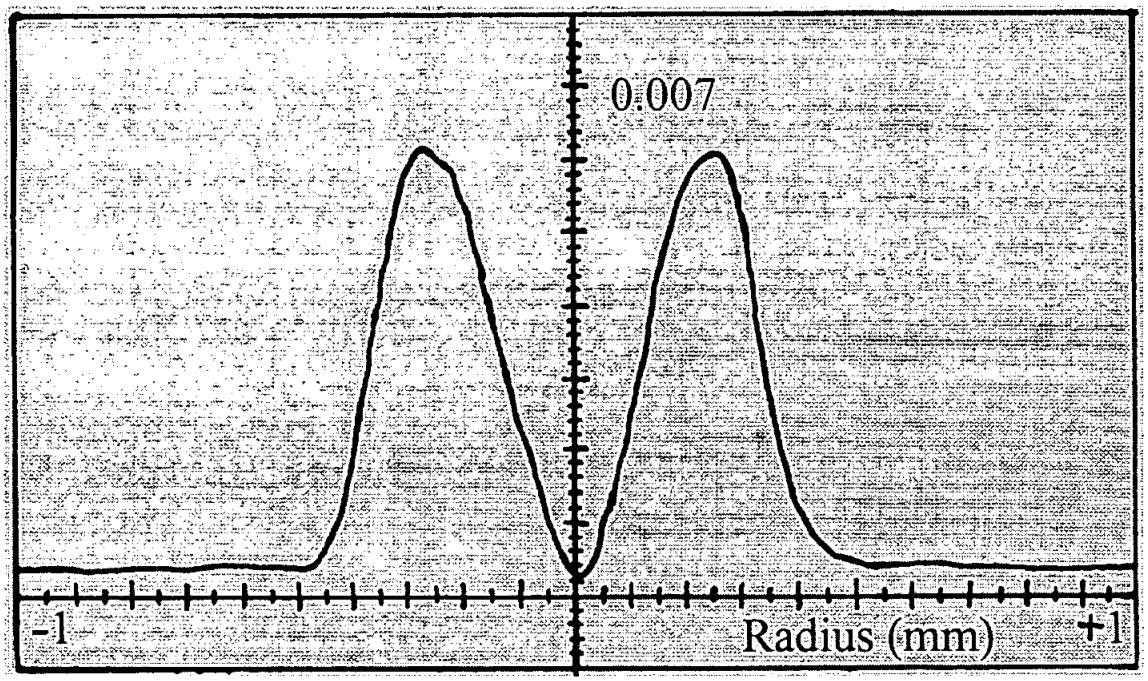

Fig. 2

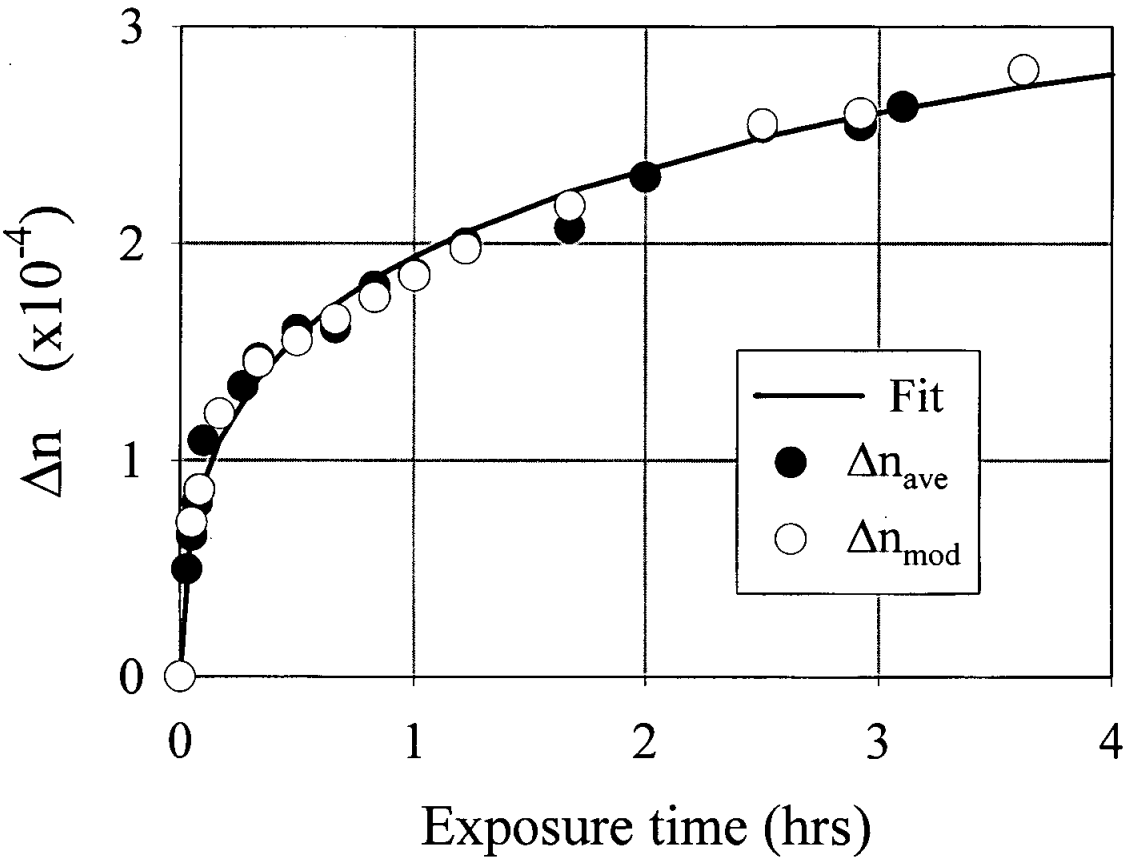

Fig. 3

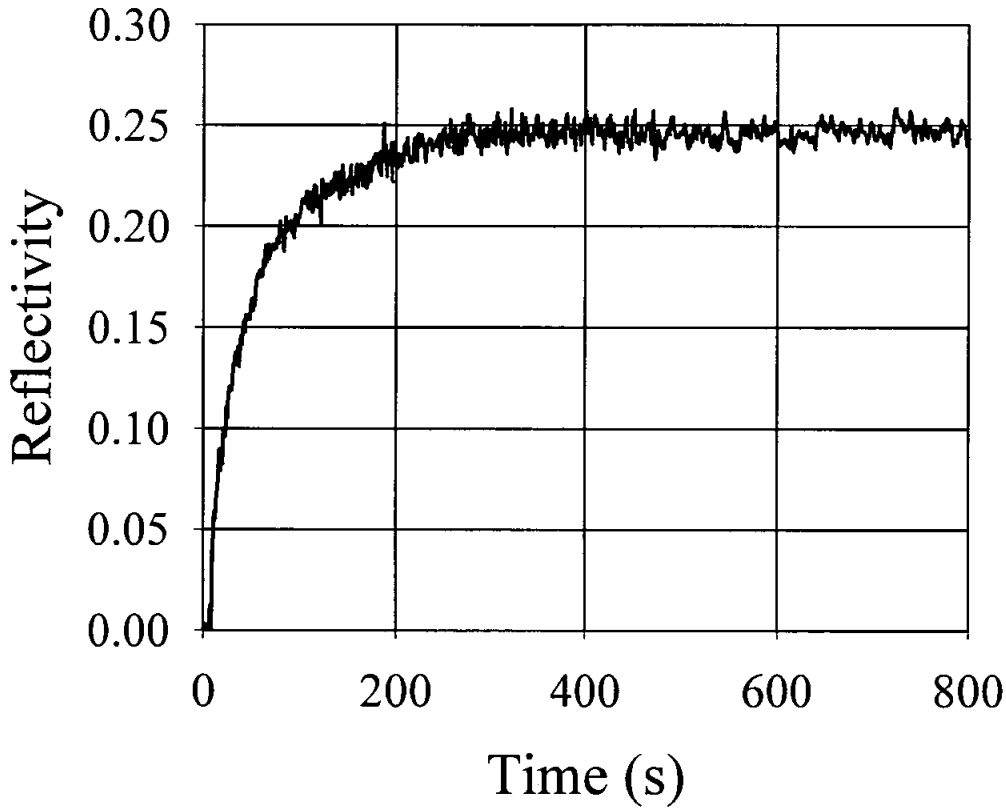
0.30
0.25
0.20
0.15
0.10
0.05
0.00
Reflectivity
0
200
400
600
800
Time (s)

Fig. 4

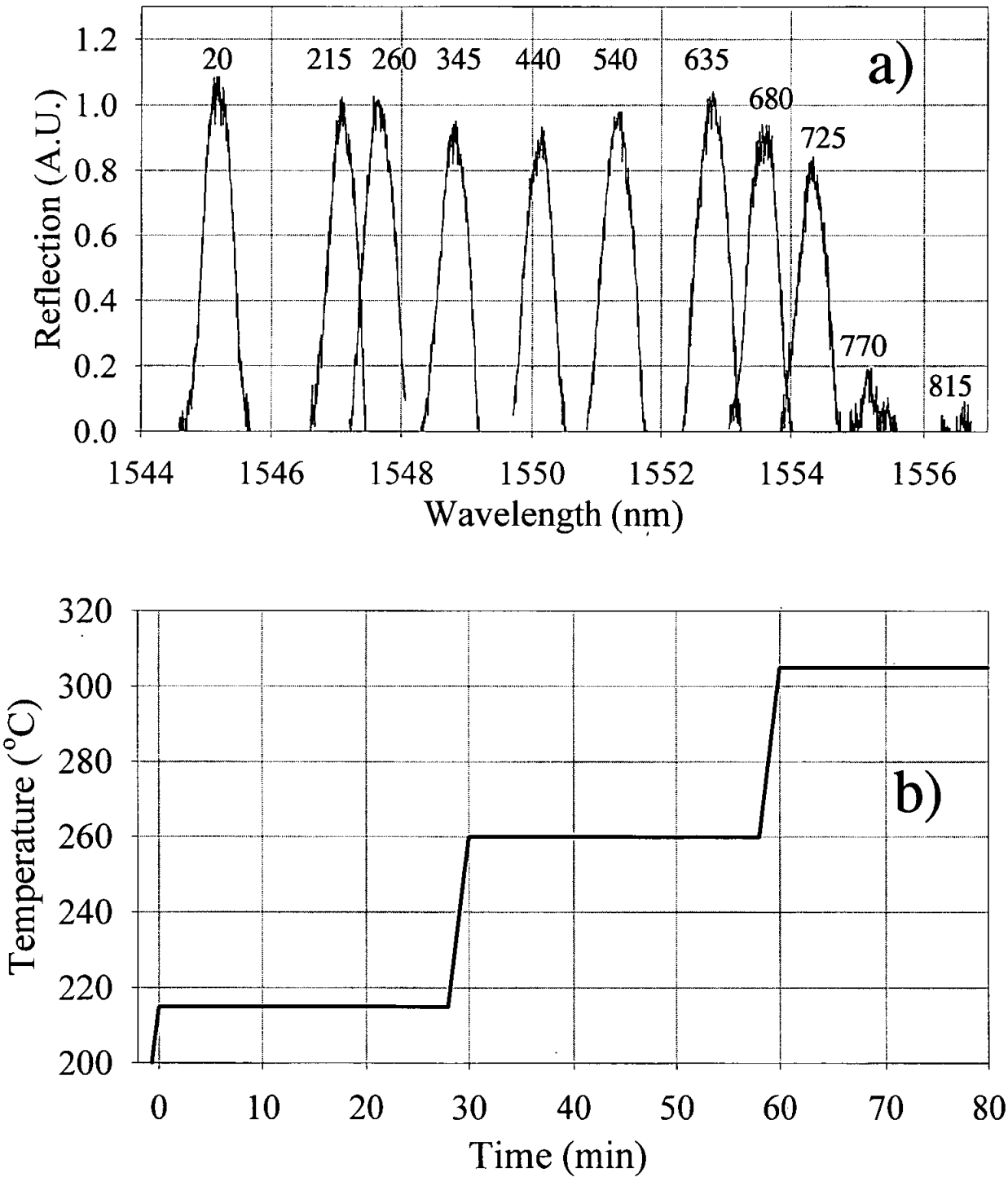
a)
20
215
260
345
440
540
635
680
725
770
815
Reflection (A.U.)
Wavelength (nm)
b)
Temperature (°C)
Time (min)

Fig. 5

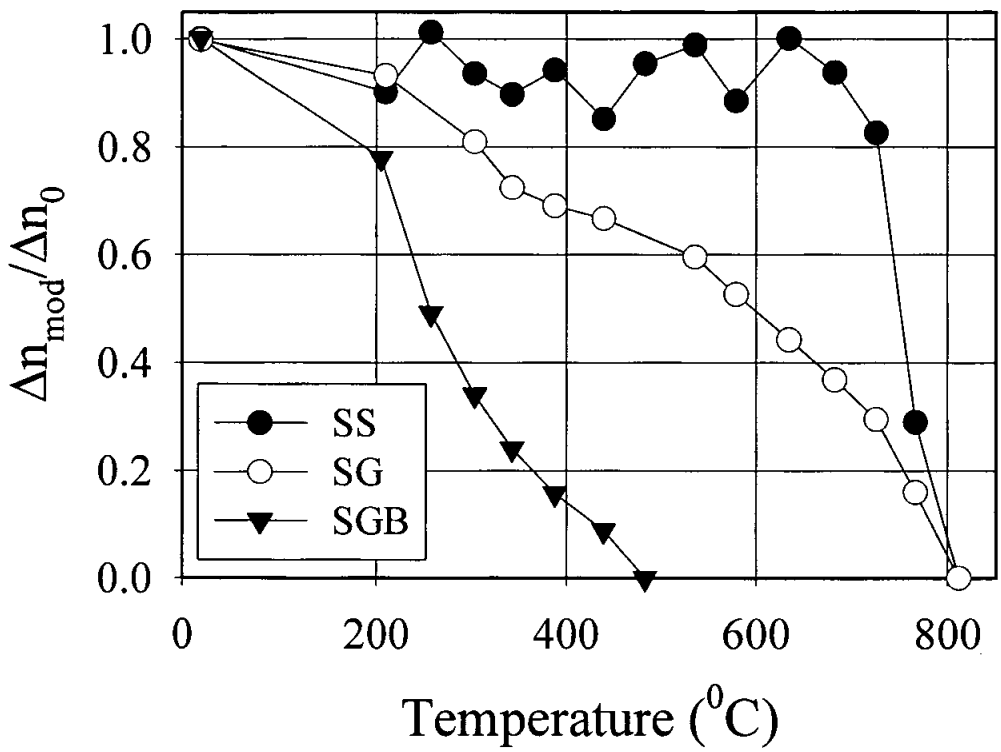
1.0
0.8
0.6
0.4
0.2
0.0
$\Delta n_{mod}/\Delta n_0$
SS
SG
SGB
0
200
400
600
800
Temperature (^{0}C)

Fig. 6

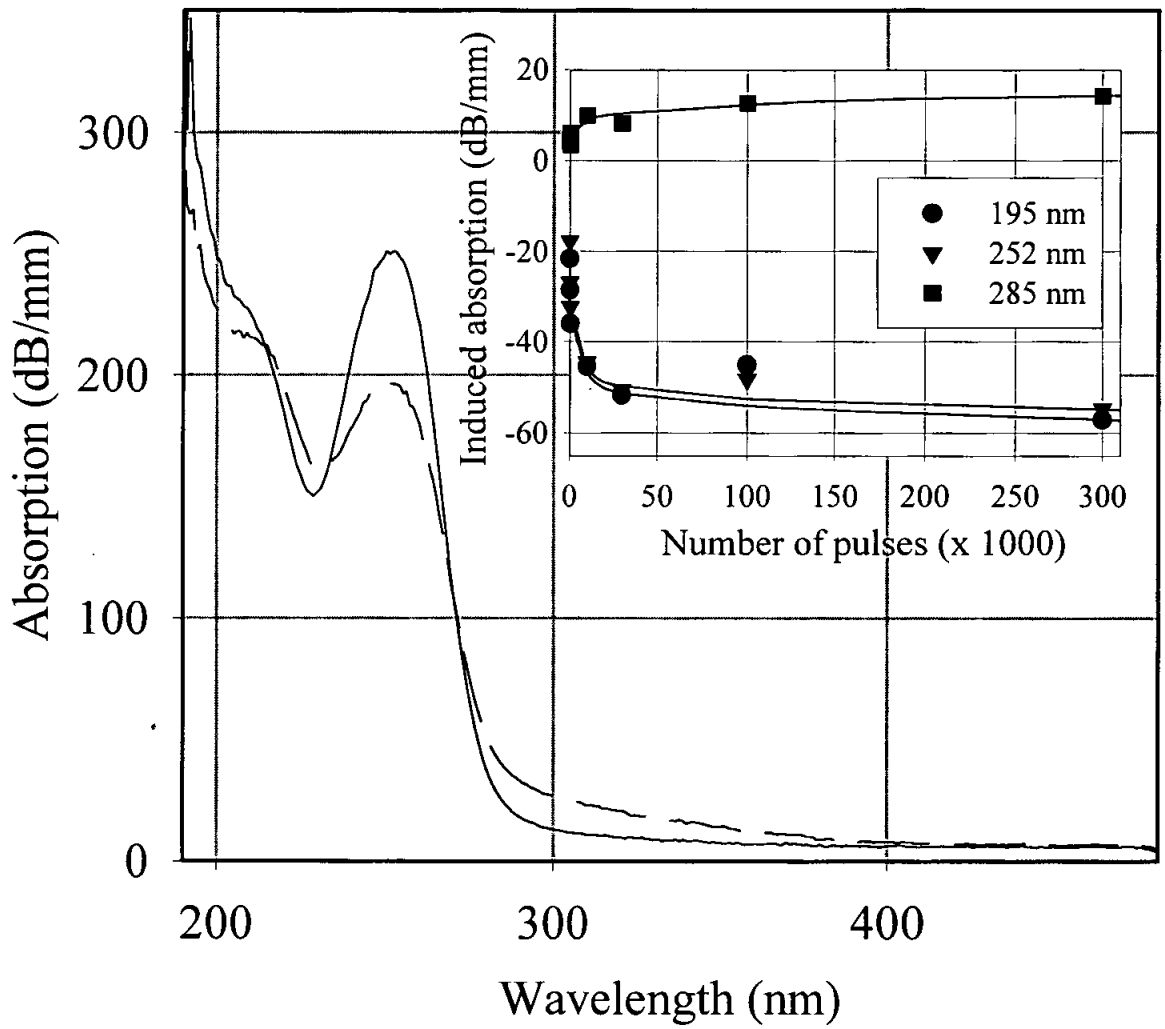
Absorption (dB/mm)
300
200
100
0
200
300
400
Wavelength (nm)
Induced absorption (dB/mm)
20
0
-20
-40
-60
0
50
100
150
200
250
300
Number of pulses (x 1000)
195 nm
252 nm
285 nm

Fig. 7

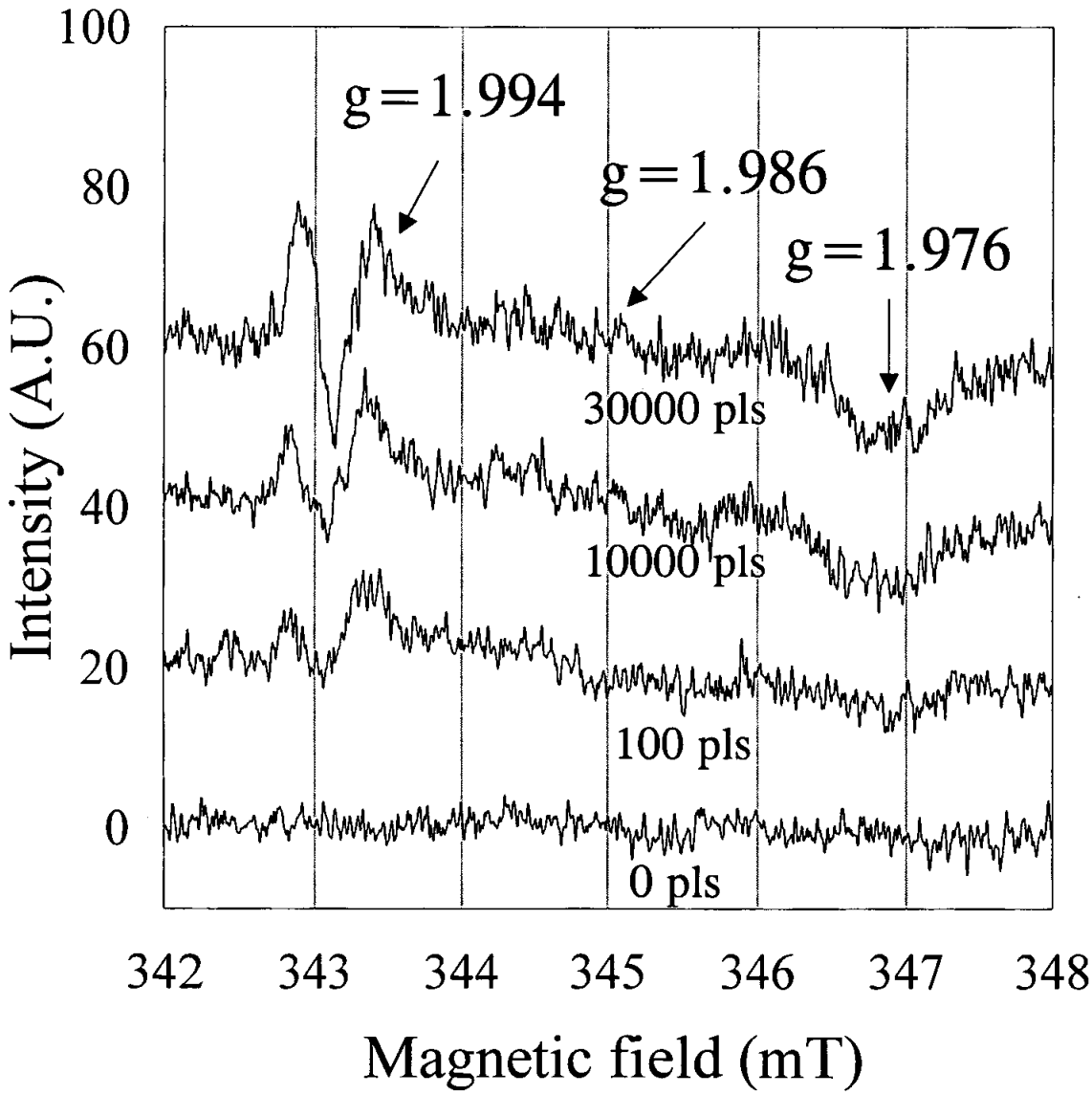
100
80
60
40
20
0
Intensity (A.U.)
g=1.994
g=1.986
g=1.976
30000 pls
10000 pls
100 pls
0 pls
342
343
344
345
346
347
348
Magnetic field (mT)

Fig. 8

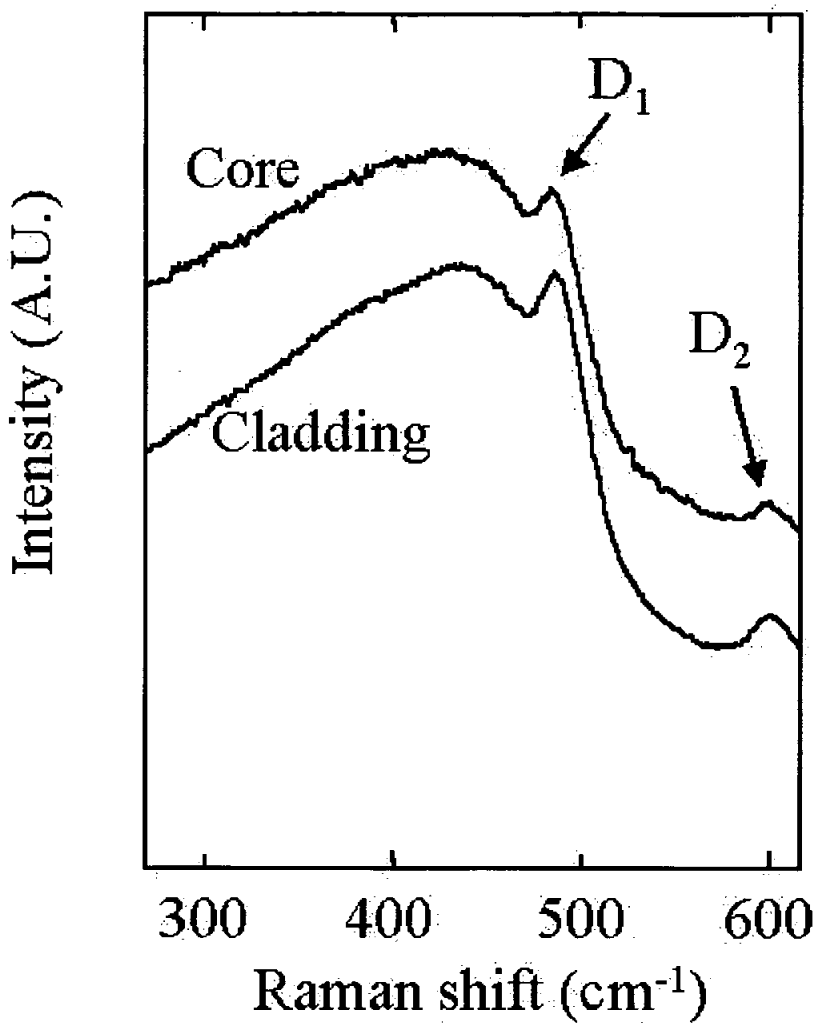
D1
Core
D2
Cladding
Intensity (A.U.)
300
400
500
600
Raman shift (cm-1)